

## Science Results Enabled by SDSS Astrometric Observations

Željko Ivezić<sup>1</sup>, Nicholas Bond<sup>2</sup>, Mario Jurić<sup>2</sup>, Jeffrey A. Munn<sup>3</sup>, Robert H. Lupton<sup>2</sup>, Jeffrey R. Pier<sup>3</sup>, Gregory S. Hennessy<sup>4</sup>, Gillian R. Knapp<sup>2</sup>, James E. Gunn<sup>2</sup>, Constance M. Rockosi<sup>5</sup>, Tom Quinn<sup>1</sup>

<sup>1</sup>*University of Washington*, <sup>2</sup>*Princeton University*, <sup>3</sup>*USNO Flagstaff*,  
<sup>4</sup>*USNO Washington D.C.*, <sup>5</sup>*University of California–Santa Cruz*

**Abstract.** We discuss several results made possible by accurate SDSS astrometric measurements in a large sky area, with emphasis on asteroids and stellar proper motions obtained by comparing POSS and SDSS. SDSS has observed over 200,000 moving objects in five photometric bands, corresponding to about two orders of magnitude increase over previous multi-color surveys. These data were used to extend the measurement of asteroid size distribution to a smaller size limit, to demonstrate that asteroid dynamical families, defined as clusters in orbital parameter space, also strongly segregate in color space, and to discover a correlation between asteroid age and colors. A preliminary analysis of SDSS-POSS proper motions for  $\sim 1$  million M dwarf stars demonstrates that, in the 0.1–1 kpc distance range, the rotational velocity and its dispersion for disk stars increase with the distance from the Galactic plane.

### 1. Introduction

The astrometric observations obtained by modern massive digital sky surveys, such as SDSS, 2MASS, and FIRST, are enabling studies that have not been possible before. In this contribution we describe several science results enabled by SDSS astrometric observations, with emphasis on observations of asteroids and proper motions obtained by comparing POSS and SDSS astrometric measurements.

The Sloan Digital Sky Survey (SDSS) is currently mapping one quarter of the sky in five optical bands (*ugriz*, Fukugita et al. 1996; Gunn et al. 1998) to a depth of  $r \sim 22.5$ , accurate to 0.02 magnitudes (both absolute calibration, and root-mean-square scatter for sources not limited by photon statistics; Ivezić et al. 2004). Astrometric positions are accurate to better than 0.1'' per coordinate (rms) for sources with  $r < 20.5$  (Pier et al. 2003), and the morphological information from the images allows reliable star/galaxy separation to  $r \sim 21.5$  (Lupton et al. 2002). The survey's coverage of  $\sim 10^4$  deg<sup>2</sup> in the North Galactic Cap and of  $\sim 200$  deg<sup>2</sup> in the Southern Galactic Hemisphere will result in photometric and astrometric measurements for over  $10^8$  stars and a similar number of galaxies. Additionally, SDSS will obtain spectra for over  $10^6$  objects, including  $10^6$  galaxies and  $10^5$  quasars. The recent third public Data Release (DR3) includes imaging data for 5282 deg<sup>2</sup> of sky, and catalogs  $1.4 \times 10^8$  objects (Abazajian et al. 2005). A detailed technical description of SDSS is given by Stoughton et al. (2002).

The SDSS astrometric reductions, and the measurements of their success, are described in detail by Pier et al. (2003). Briefly, the SDSS absolute astrometric accuracy is better than 100 mas, with relative (band-to-band) accuracy of about 20-30 mas (rms, for sources not limited by photon statistics). In addition to providing positions for a large number of objects with a remarkable accuracy (and thus enabling recalibration of other less accurate surveys, as described below), an important characteristic of SDSS astrometric observations is that measurements in five photometric bands are obtained over a five minute long period (with 54 sec per exposure). The multi-color nature allows the discovery of the so-called Color Induced Displacement binary stars (for details see Pourbaix et al. 2004), and the time delay allows the recognition of moving objects, discussed next.

## 2. SDSS Observations of Solar System Objects

Although primarily designed for observations of extragalactic objects, the SDSS is significantly contributing to studies of solar system objects, because asteroids in the imaging survey must be explicitly recognized to avoid contamination of the quasar samples selected for spectroscopic observations (Lupton *et al.* 2002). The SDSS has already increased the number of asteroids with accurate five-color photometry by about two orders of magnitude (to over 200,000), and to a limit more than five magnitudes fainter than previous multi-color surveys (Ivezić *et al.* 2001).

About 43,000 of those 200,000 objects have been associated with previously known asteroids that have well determined orbital elements (Jurić *et al.* 2002). Both SDSS data and orbital elements are available from the public SDSS Moving Object Catalog<sup>1</sup> (Ivezić *et al.* 2002a). The SDSS observations of objects with known orbits vividly demonstrate that asteroid dynamical families, defined as clusters in orbital parameter space, also strongly segregate in color space (Ivezić *et al.* 2002b). This segregation indicates that the variations in chemical composition within a family are much smaller than the compositional differences between families, and strongly support earlier suggestions that asteroids belonging to a particular family have a common origin.

Asteroid colors measured by SDSS are well correlated with the family age (Jedicke *et al.* 2004), which provides a direct evidence for space weathering, and offers a method to date asteroids using their SDSS colors. The effects of space weathering can also explain the color variability of asteroids measured by SDSS (Szabo *et al.* 2004).

## 3. Proper Motions Determined from SDSS and POSS Observations

Munn *et al.* (2004, hereafter M04) have recently presented an improved proper-motion catalog for  $\sim 8$  million stars, based on combining the USNO-B and SDSS catalogs in the 2099 deg<sup>2</sup> large area of sky covered by SDSS Data Release 1. USNO-B positions are recalibrated using SDSS galaxies, which results in smaller

---

<sup>1</sup>Available from [http://www.sdss.org/dr2/products/value\\_added/index.html](http://www.sdss.org/dr2/products/value_added/index.html)

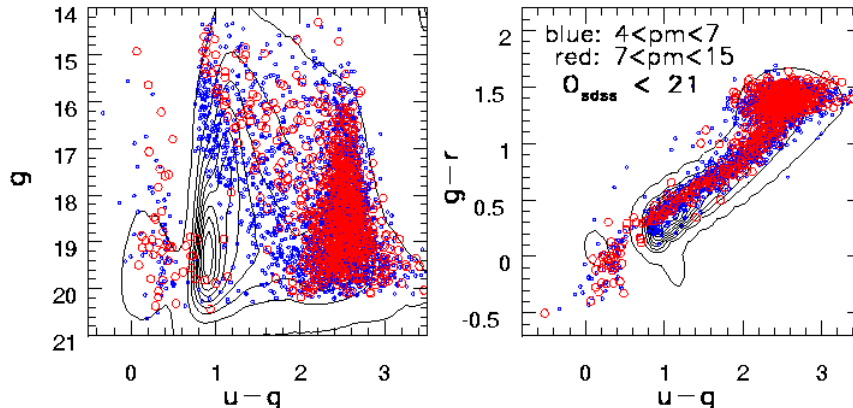


Figure 1. An illustration of the differences in the distribution of point sources in SDSS color-magnitude and color-color diagrams induced by requiring a large proper motion. The distribution of all point sources is shown by contours, and two subsets of sources with large proper motion are shown by symbols (small: 4–7 mas/yr; large: 7–15 mas/yr). The white dwarfs are easily recognized by their blue  $u - g$  color ( $u - g < 0.8$ ), while the majority of other sources with large proper motions are main sequence stars. M dwarfs, at distances up to  $\sim 1$  kpc, dominate the large proper motion sample.

astrometric errors and the placement of proper motions on an absolute reference frame. Tests based on several tens of thousand quasars spectroscopically confirmed by SDSS show that the proper motion errors are  $\sim 3$  mas/yr for bright ( $g < 18$ ) sources (rms per coordinate), with substantially smaller systematic errors ( $< 0.5$  mas/yr, and typically  $\sim 0.1$  mas/yr), and excellent stability across the sky. For fainter sources, the proper motion errors increase to  $\sim 4$  mas/yr at  $g \sim 19$ ,  $\sim 5.7$  mas/yr at  $g \sim 20$ , and to  $\sim 7.5$  mas/yr at  $g \sim 20.5$ , the faint limit for the sample discussed here. For stars at 500 pc, these proper motion errors correspond to systematic velocity error of  $< 1$  km/s, and to random velocity errors of 7 km/s at the bright end (without including errors in distance), and 20 km/s at the faint end.

This accurate proper motion database offers numerous possibilities for studying the stellar kinematics, but the analysis of such a large and highly-dimensional data set is not trivial. At the very least, the proper motion components are functions of at least four observables: apparent magnitude, distance (or absolute magnitude, measured by e.g.  $r - i$  color), and the position on the sky (Fig. 1). Additional stellar parameters, such as metallicity (measured from spectra, or estimated from the  $u - g$  color), are also expected to play a role. Furthermore, the probed distance range is large (out to  $\sim 15$  kpc with main sequence stars, Jurić et al. 2005) and thus the dependence of the stellar velocity distribution on position in the Galaxy could also be important, as well as the deviations from a Gaussian distribution.

In this contribution we limit our analysis to M dwarfs from the M04 proper motion catalog because 1) they dominate the high proper motion sample, and 2) their distances can be reliably determined from a photometric parallax relation. A more comprehensive analysis of that catalog, that also includes three-

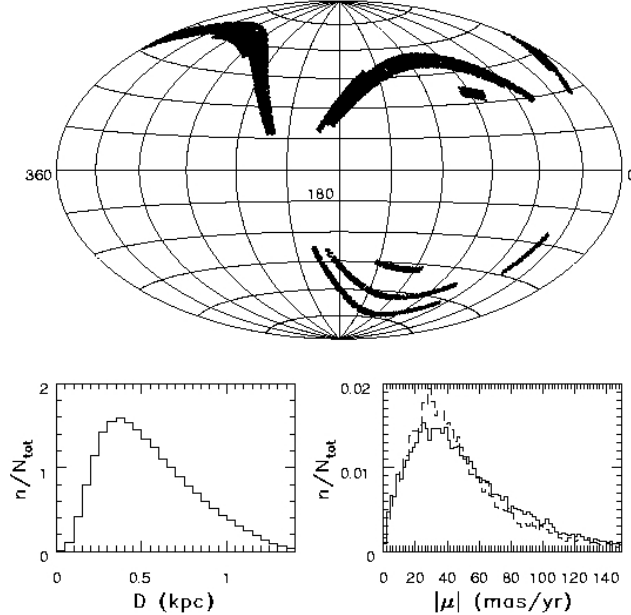


Figure 2. The bottom left panel shows the distance distribution for a sample of 881,913 M dwarfs with SDSS-POSS proper motions. The top panel shows the sky distribution for a subsample with distances in the range 100–150 pc in Aitoff projection of galactic coordinates, and the bottom right panel compares the proper motion distribution for this subsample before (solid) and after (dashed) correction for solar peculiar motion (see § 3.1.).

dimensional velocities for  $\sim 100,000$  stars with SDSS spectra, will be presented by Bond et al. (2005, in prep., hereafter B05).

We select 881,913 M dwarfs from the M04 catalog by requiring  $1.25 < g - r < 1.50$ ,  $0.6 < r - i < 1.6$  and  $15 < g < 20.5$  (Ivezić et al. 2004), and estimate their distances using a photometric parallax relation:

$$M_i = 4.0 + 10.86(r - i) - 10.74(r - i)^2 + 5.99(r - i)^3 - 1.20(r - i)^4. \quad (1)$$

These distances have random errors of  $\sim 10\%$ , with comparable systematic errors (Jurić et al. 2005). The sky and distance distributions of selected stars are shown in Fig. 2. The size of this sample and its sky distribution make it well suited for a determination of solar peculiar motion, discussed next.

### 3.1. Determination of Solar Motion Relative to M dwarfs

The solar peculiar motion with a magnitude of  $v_\odot$ , induces a dipole in the proper motion distribution for sources at a distance  $D$ , with a magnitude of  $\sim 3.2 (v_\odot/15 \text{ km/s}) (\text{kpc}/D) \text{ mas/yr}$ , which is easily measurable with the sample discussed here. We follow a procedure outlined by Mihalas & Binney (1981), and determine the apex coordinates and the magnitude of implied solar motion for subsamples selected in narrow distance bins (Fig. 3).

The extrapolation of results shown in Fig. 3 to zero distance gives ( $l_A=68^\circ$ ,  $b_A=32^\circ$ , and  $v_A=9 \text{ km/s}$ ), somewhat different from standard values ( $l_A=51^\circ$ ,  $b_A=23^\circ$ , and  $v_A=15 \text{ km/s}$ ; Mihalas & Binney 1981). However, as evident from Fig. 3, all three quantities vary as a function of the subsample distance. We find

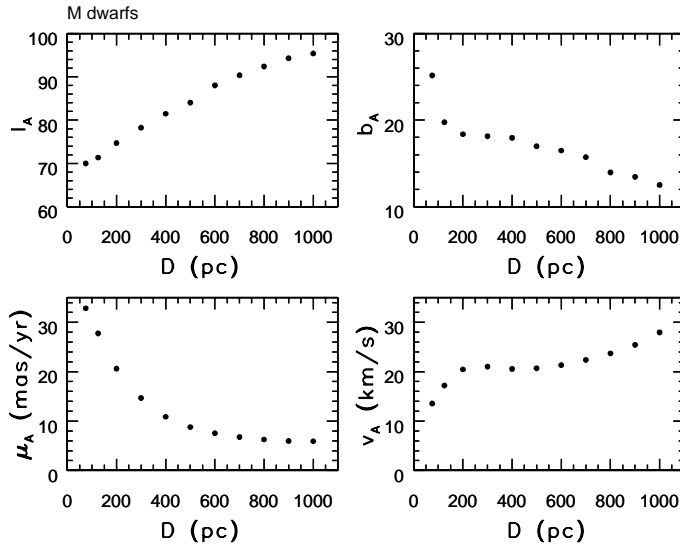


Figure 3. The galactic coordinates of the solar apex (the top two panels), implied proper motion magnitude (bottom left), and corresponding solar velocity (bottom right), determined as a function of distance using SDSS-POSS proper motions for a sample of 881,913 M dwarfs.

that this effect is caused by the increase of the rotational velocity component with the distance from the plane, which breaks the dipole assumption of the Mihalas & Binney method. Consequently, the apex is biased toward ( $l \sim 90^\circ$ ,  $b_A = 0^\circ$ ) direction, with a corresponding increase of  $v_A$ . An illustration of this dependence is discussed next. Additional supporting evidence for this claim, which utilizes three-dimensional velocity information, will be described in N05.

### 3.2. Kinematics as a Function of $Z$

Here we present results for the kinematics of M dwarfs observed towards the Galactic anticenter. In this direction, the rotational velocity is dominated by the longitudinal velocity component measured from proper motion, and thus robust results can be derived without radial velocity information. The top two panels in Fig. 4 show the dependence of longitudinal and latitudinal velocity components, determined from proper motions, for  $\sim 50,000$  M dwarfs toward  $l \sim 180$  (without including correction for solar peculiar motion, which amounts to an overall shift of the longitudinal component by  $\sim 10$  km/s). While the median values of the latitudinal component are assuringly consistent with zero, the medians of the longitudinal component increase with the distance from the plane,  $Z$ , as  $v_l = (12 + 22 |Z/\text{kpc}|^{1.3})$  km/s (with the uncertainty of  $\sim 10\%$  for all three fitted parameters).

From the data presented here it cannot be ruled out that the observed variation of  $v_l$  actually reflects a dependence on the radial distance from the Galactic center (because the range of galactic latitudes observed by SDSS towards  $l \sim 180$  is limited). However, N05 demonstrate, using three-dimensional velocity information, that the  $Z$  dependence dominates. Furthermore, they also show that the same relation describes the behavior of  $v_l$  for bluer stars that sample distances out to  $\sim 3$  kpc (though with less reliable distances).

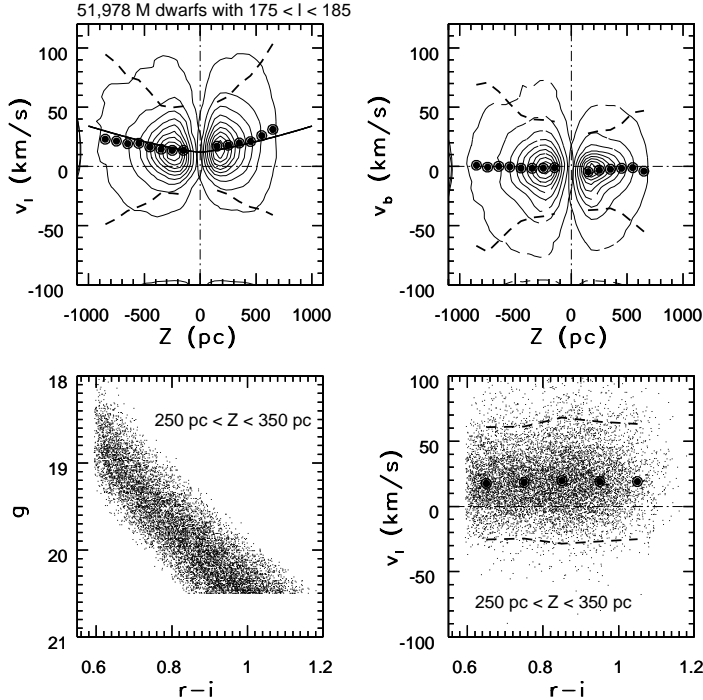


Figure 4. The contours in the top left panel show the longitudinal velocity component determined from proper motion measurements,  $v_l$ , as a function of distance from the Galactic plane,  $Z$ , for 51,978 M dwarfs with  $175 < l < 185$ . Toward this direction, the longitudinal velocity is equivalent to rotational velocity. The large dots are the median values of  $v_l$  for a given  $Z$  bin. The dashed lines represent  $2\sigma$  envelope around the median ( $\sigma$  is determined using the interquartile range). The line following the medians is  $v_l = (12 + 22 |Z/\text{kpc}|^{1.3})$  km/s. The top right panel is analogous, except that the latitudinal velocity component is shown. The bottom left panel shows the  $g$  vs.  $r - i$  color-magnitude diagram for a subsample of 9,231 stars with  $250 < Z/\text{pc} < 350$ . The longitudinal velocity component of those stars as a function of  $r - i$  color is shown in the bottom right panel, with the same meaning of symbols and lines as in the top two panels. Note that neither the median, nor the distribution width, vary with color, although the apparent magnitude,  $g$ , varies by  $\sim 2$  mag.

### 3.3. The Shape of the Velocity Distribution

The analysis described in preceding sections considers only the first two moments of the velocity distribution. Nevertheless, the large number of stars allows an unprecedentedly robust and accurate analysis of the full shape of the velocity distribution. As Figs. 5 and 6 show, the observed shapes significantly deviate from Gaussian, and show distortions similar to those expected from the asymmetric drift effect (Mihalas & Binney 1981). The shapes also vary with distance, a variation that is hard to explain as due to increasing proper motion errors toward the faint end (Fig. 6). The observations of the shape of the velocity distribution, and its dependence on the position and stellar tracer, encode an enormous amount of information (e.g. Binney & Tremaine 1987) that we are only beginning to harvest.

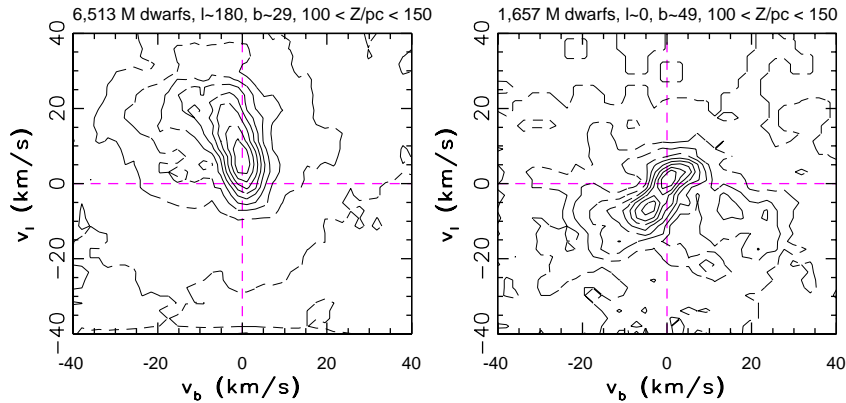


Figure 5. The two-dimensional velocity distribution,  $v_l$  vs.  $v_b$ , determined from proper motion measurements for two characteristic lines of sight (left:  $175 < l < 185$ , right:  $355 < l < 5$ ) and for the height above the plane in the range 100–150 pc. The density of sources is shown by linearly spaced isopleths.

#### 4. Discussion

The availability of modern massive sky surveys is rapidly changing astronomical methodology, and enables studies that were not possible until recently. This is particularly true for astrometric data provided by SDSS. A good example is the SDSS observations of asteroids: in only a few years, the SDSS has increased the sample of asteroids with accurate colors by about two orders of magnitude, and enabled detailed and robust studies of correlations between asteroid chemical and dynamical properties.

Another example where SDSS data were crucial is the construction of the Munn et al. SDSS-POSS proper motion catalog. This resource is bound to make significant contributions to our understanding of the Milky Way kinematics. The preliminary results discussed here suggest that these kinematics may be significantly more complex than assumed until now.

**Acknowledgments.** Funding for the creation and distribution of the SDSS Archive has been provided by the Alfred P. Sloan Foundation, the Participating Institutions, the National Aeronautics and Space Administration, the National Science Foundation, the U.S. Department of Energy, the Japanese Monbukagakusho, and the Max Planck Society. The SDSS Web site is <http://www.sdss.org/>.

#### References

- Abazajian, K., Adelman-McCarthy, J.K., Agüeros, M.A., et al. 2005, *AJ*, in press  
 Binney, J. & Tremaine S. 1987, *Galactic Dynamics* (Princeton: Princeton Univ. Press)  
 Fukugita, M., Ichikawa, T., Gunn, et al. 1996, *AJ*, 111, 1748  
 Gunn, J.E., Carr, M., Rockosi, C., et al. 1998, *AJ*, 116, 3040  
 Ivezić, Ž., Tabachnik, S., Rafikov, R., et al. 2001, *AJ*, 122, 2749  
 Ivezić, Ž., Jurić, M., Lupton, R.H., et al. 2002a, *astro-ph/0208099*

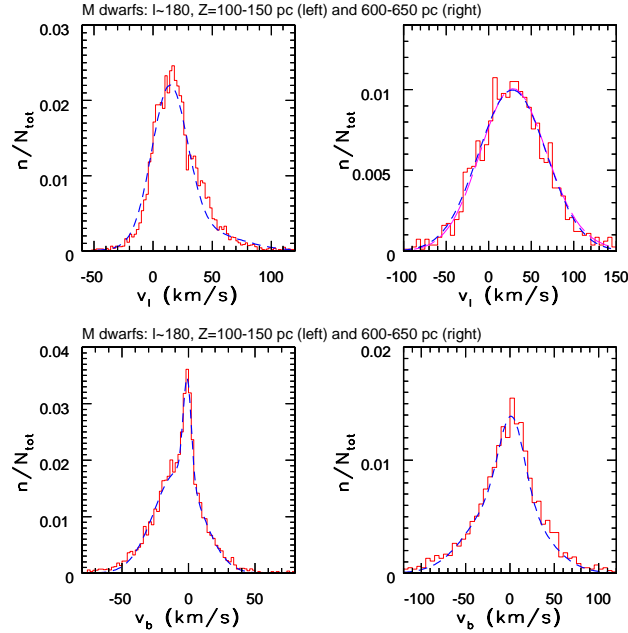


Figure 6. An analysis of the shape of the  $v_l$  (top) and  $v_b$  (bottom) distributions toward  $l \sim 180$ , and for two ranges of distance from the Galactic plane (left: 100–150 pc, corresponding to the left panel in Fig. 5, right: 600–650 pc). The histograms shown by thin full lines are the data for 7,042 (left) and 1,705 (right) stars, and the dashed lines show empirical models. In the top left panel, the model is a sum of two Gaussians  $(\mu, \sigma) = (14, 15)$  and  $(38, 34)$  km/s, with the wider component accounting for 43% of the sample. In the top right panel, the short-dashed line is a Gaussian with  $(\mu, \sigma) = (28, 40)$  km/s, and the thin long-dashed line (almost indistinguishable) is the convolution of the data shown in the top left panel with a  $(\mu, \sigma) = (0, 34)$  km/s Gaussian, and shifted right by 10 km/s. Since the expected measurement errors are much smaller (random  $\sim 21$  km/s, and systematic  $< 1$  km/s), they cannot explain the observed change of the  $v_l$  distribution shape as the distance increases from 100 to 600 pc. In the bottom left panel, the model is a sum of two Gaussians  $(\mu, \sigma) = (-1, 3)$  and  $(-8, 18)$  km/s, with the wider component accounting for 86% of the sample. In the bottom right panel, the model is a sum of two Gaussians  $(\mu, \sigma) = (2, 14)$  and  $(-5, 38)$  km/s, with the wider component accounting for 73% of the sample.

- Ivezić, Ž., Lupton, R.H., Jurić, M., et al. 2002b, *AJ*, 124, 2943  
 Ivezić, Ž., Lupton, R.H., Schlegel, D., et al. 2004, *AN*, 325, No. 6-8, 583  
 Jedicke, R., Nesvorný, D., Whiteley, R., Ivezić, Ž., Jurić, M. 2004, *Nature*, 429, 275  
 Jurić, M., Ivezić, Ž., Lupton, R.H., et al. 2002, *AJ*, 124, 1776  
 Lupton, R.H., Ivezić, Ž., Gunn, J.E., et al. 2002, in “Survey and Other Telescope Technologies and Discoveries”, Tyson, J.A. & Wolff, S., eds. SPIE 4836, 350  
 Mihalas, D. & Binney, J. 1981, *Galactic Astronomy* (San Francisco: W.H. Freeman)  
 Munn, J.A., Monet, D.G., Levine, S.E., et al. 2004, *AJ*, 127, 3034  
 Pier, J.R., Munn, J.A., Hindsley, R.B., et al. 2003, *AJ*, 125, 1559  
 Pourbaix, D., Ivezić, Ž., Knapp, G.R., Gunn, J.E., Lupton, R.H. 2004, *A&A*, 423, 755  
 Stoughton, C., Lupton, R.H., Bernardi, M., et al. 2002, *AJ*, 123, 485  
 Szabo, Gy.M., Ivezić, Ž., Jurić, M., Lupton, R.H. & Kiss, L.L. 2004, *MNRAS* 348, 987  
 York, D.G., Adelman, J., Anderson, S., et al. 2000, *AJ*, 120, 1579